Modeling Aging of Displacement Piles in Natural Soft Clay

Modeling Aging of Displacement Piles in Natural Soft Clay

Mats Karlsson, Ph.D.[1]; Jorge Yannie, Ph.D.[2]; and Jelke Dijkstra[3]

Abstract: A multitude of mechanisms will affect the evolution of the pile response over time, each with their respective time scale. It is shown that most of the processes can be linked to the pile installation stage, which alters the soil surrounding the pile. As a result, there is a change in the mechanical properties of the soil that will influence the subsequent pile response over time. These long-term mechanisms include the dissipation of excess pore pressures from pile installation and the creep in the soil. This paper presents a numerical approach that combines the strain-path method, an advanced effective stress–based constitutive model for soft soils, and a multiphase numerical framework that enables the modeling of the pile installation and subsequent change of pile bearing capacity over time. The presented results demonstrate that the degree of remolding of the soil during the pile installation stage is closely linked to the subsequent pile response. For the Onsøy test case studied, the increase in shaft capacity over time, demonstrated to be linked to undrained strength recovery, could be faithfully reproduced during and after dissipation of excess pore pressures. Hence, pile aging of displacement piles installed in clay is strongly linked to installation effects and the creep and relaxation processes in the soil. Further study is required to fully reveal the physicochemical mechanisms that underpin these processes. **DOI: 10.1061/(ASCE)GT.1943-5606.0002110.**

Author keywords: Pile installation; Pile setup; Pile aging; Creep.

Introduction

There is renewed interest in recent years in the gain of bearing capacity in both sands and clays (e.g., Lehane and Jardine 1994; Chow et al. 1998; Axelsson 2000; Hunt et al. 2002; Bullock et al. 2005a, b; Fellenius 2008; Karlsrud et al. 2014; Lim and Lehane 2014; Haque et al. 2016). The numerical efforts so far have been focused on the pile-setup stage (e.g., Randolph et al. 1979; Whittle and Sutabutr 1999; Basu et al. 2014; Abu-Farsakh et al. 2015), linking the (undrained) pile installation and dissipation of excess pore pressures. Reliable experimental studies on pile setup are scarce because the load needs to be applied for long periods of time, and the pile should be loaded to failure during the pile load test. Alternatively, in less rigorous tests, pile-setup effects are studied for unloaded piles where the same pile is dynamically (or statnamically) tested at several instances in time, and sometimes fresh piles are tested using these faster pile-loading methods. The latter type of pile load tests are rate-dependent (i.e., emerging stiffness and strength varies as function of strain rate), which potentially influences the results, especially in clays. As such, the tests performed by Karlsrud et al. (2014) are of most interest here because not only were the piles tested using static pile load tests, but also some of the piles were loaded during the pile setup and subsequent pile-aging period. In addition, a well-documented test site, i.e., Onsøy, was used.

Generally, the increase in pile capacity over time after pile installation is referred to as setup (Fleming et al. 2008). The main mechanism is the dissipation of excess pore-water pressures that were generated during pile installation. The setup phase includes (1) recovery of effective stress due to the dissipation of excess pore-water pressures, and (2) the change in strength independent of the dissipation of pore-water pressures. Some of the second type of mechanisms both start and finish during pile setup, such as thixotropy in clays (Seng and Tanaka 2012), whereas others continue after the dissipation of pore-water pressures (and hence setup) has already finished. In this ongoing phase, stress-relaxation and creep mechanisms in the soil surrounding the pile shaft continue to influence the mobilized pile capacity. These ongoing processes with time are sometimes referred to as aging effects and are, among others, linked to grain-level mechanisms such as contact aging and breakage in sands (Schmertmann 1991; Michalowski and Nadukuru 2012) and thixotropy in clay (Seng and Tanaka 2012). The time scales of these processes differ largely between sand and clay given that thixotropy in clay is shorter than contact aging effects in sand. It, therefore, is postulated that for pile aging of displacement piles in natural soft clays, thixotropy is not the governing mechanism. Rather a combination of creep and relaxation in the soil is affecting the pile response most.

The link with pile installation suggests that the process is largely a strength-recovery process from the disturbances of pile installation, rather than a principal gain in capacity only (e.g., Lim and Lehane 2014). Therefore, the process is not as often studied numerically because the soil disturbances from the installation process need to be incorporated in the analyses. For clays, perhaps the most complete attempt was presented by Abu-Farsakh et al. (2015), where installation effects, soil anisotropy, and thixotropy (on the interface) were incorporated in the analyses. The traditional empirical interpretation of the pile setup phase that includes dissipation of excess pore pressures, thixotropy in clay, and other unidentified time-dependent mechanisms still mainly revolves around fitting dimensionless setup factors (Yang and Liang 2006), such as those originally proposed by Skov and Denver (1988).

[1]Div. of Geology and Geotechnics, Chalmers Univ. of Technology, Gothenburg SE-41296, Sweden. Email: mats.karlsson@chalmers.se

[2]Div. of Civil Engineering, NCC Infrastructure, Vallgatan 3, Solna SE-17080, Sweden. Email: jorge.yannie@ncc.se

[3]Professor, Div. of Geology and Geotechnics, Chalmers Univ. of Technology, Gothenburg SE-41296, Sweden (corresponding author). ORCID: https://orcid.org/0000-0003-3792-0727. Email: jelke.dijkstra@chalmers.se

Note. This manuscript was submitted on May 14, 2018; approved on March 15, 2019; published online on July 26, 2019. Discussion period open until December 26, 2019; separate discussions must be submitted for individual papers. This paper is part of the ***Journal of Geotechnical and Geoenvironmental Engineering***, © ASCE, ISSN 1090-0241.

The current work aims to advance the understanding off the pile-aging process in clays by incorporating the pile installation, subsequent consolidation, and creep in the analyses. The hypothesis is that a significant part of the pile aging is simply linked to the creep and relaxation processes in the soft clay, which is affected by the effective stress history from pile installation and subsequent consolidation. This requires a novel combination of the strain-path method to model pile installation, and a constitutive model for soft soils that includes creep to quantify pile aging. The proposed method will be validated for a well-documented field test on the Onsøy test site (Karlsrud et al. 2014).

Methodology

Constitutive Model

A constitutive model that incorporates creep and relaxation (in constitutive terms, often referred to as rate-dependence) is required in order to capture the time-dependent nature of the pile-aging process. Hence, the constitutive soil model used in the numerical analyses is the Creep-SCLAY1S model (Sivasithamparam et al. 2015; Gras et al. 2017, 2018), which is a viscoplastic model that incorporates the following features:

- Rate-dependency (creep): this includes the ability to capture (tertiary) creep phenomena as well as stress relaxation after pile installation.
- Anisotropy (a rotational viscoplastic hardening function): this allows better prediction of the change in soil response after excessive deformation, as well as the fact that the natural soft clays encountered at the test location are inherently anisotropic (e.g., Wichtmann et al. 2013);
- Destructuration (gradual degradation of the weak bonding, present in natural soft clays as a function of irreversible strains): this part of the model describes the significant loss of strength and stiffness after excessive deformation.

The Creep-SCLAY1S model is originally implemented in a format suitable for Abaqus (user-defined material model format UMAT), which is directly compatible with the used strain driver developed by Niemunis (2008). The Physics Builder interface was used for the model implementation in COMSOL Multiphysics version 5.3.

A full overview of the model parameters that were calibrated against a series of one-dimensional (1D) incremental loading compression tests and anisotropically consolidated triaxial tests on Onsøy clay is presented in Table 1.

Table 1. Model parameters for natural Onsøy clay

Parameter	Definition	Value
λ_i^*	Modified intrinsic compression index	0.076
κ^*	Modified swelling index	0.011
ν	Poisson's ratio	0.15
M_c	Stress ratio at critical state in triaxial compression	1.23
M_e	Stress ratio at critical state in triaxial extension	0.80
ω	Rate of rotation	200
ω_d	Rate of rotation due to deviator strain	0.56
a	Rate of destructuration	10
b	Rate of destructuration due to deviator strain	0.30
OCR	Overconsolidation ratio	1.1
e_0	Initial void ratio	1.80
α_0	Initial anisotropy	0.47
χ_0	Initial amount of bonding	10
μ_i^*	Modified intrinsic creep index	0.005
τ (days)	Reference time	1

Modeling Pile Installation

The pile installation stage is modeled using the strain-path method (SPM), which was first developed by Baligh (1985) and further expanded by Sagaseta et al. (1997) with the inclusion of shallow strain-path solutions. The original SPM formulation of Baligh (1985) only considered a deep foundation and is an approximate analytical procedure to predict soil disturbance due to installation of rigid objects in the soil. This method does not incorporate the ground surface and hence is only applicable for processes at depth where the ground surface has a negligible influence on the results. The calculated kinematics are independent of the stress-strain relations of the soil because they are based on velocity fields for incompressible and inviscid flow calculated using potential theory. The shallow strain-path method (SSPM) (Sagaseta et al. 1997) used here, however, incorporates surface effects in a rigorous fashion.

The SSPM equations are implemented in COMSOL Multiphysics version 5.3, after which the strain paths are parsed to a strain driver to obtain updated stress fields, excess pore pressure fields, and all other state variables of the constitutive model. The most challenging aspect of the SSPM implementation relates to the evaluation of the corrective shear tractions [Step 3 or Eqs. (17)–(24*a*) in Sagaseta et al. (1997)]. Here in the COMSOL implementation, the complete elliptic integrals of the first and second kind are approximated by a power series with $n = 100$ according to Eqs. (1) and (2)

$$\int_0^{2\pi} \frac{d\theta}{\sqrt{1-k^2\sin^2\theta}} = \frac{\pi}{2}\sum_{n=0}^{\infty}\left(\frac{(2n)!}{2^{2n}(n!)^2}\right)^2 k^{2n} \tag{1}$$

$$\int_0^{2\pi} \sqrt{1-k^2\sin^2\theta}\,d\theta = \frac{\pi}{2}\sum_{n=0}^{\infty}\left(\frac{(2n)!}{2^{2n}(n!)^2}\right)^2 \frac{k^{2n}}{1-2n} \tag{2}$$

where k = modulus of the approximated elliptic integral; and Θ = amplitude angle.

The (effective) stress state in the soil still is unknown after calculating the soil kinematics with the SSPM method. The complementary stress components are subsequently calculated by pointwise parsing the strain path from installation in a strain driver (Niemunis 2008) equipped with the Creep-SCLAY1S constitutive model (Sivasithamparam et al. 2015; Gras et al. 2018).

Finally, after obtaining the stress increments complementary to the strain paths for each point in the domain individually, the stress equilibrium, strain compatibility, and excess pore pressures (and their dissipation) are solved in a two-dimensional (2D) finite-element (FE) code (again COMSOL) with the Creep-SCLAY1S model. A fully coupled analysis is conducted to evaluate the consolidation and creep processes over time.

The aforementioned steps are performed to overcome the mesh distortion issues resulting from large deformations during the pile installation process and are, apart from some small differences in Step 1, equal for any type of displacement pile. The focus is on calculating the effect of pile installation on the long-term response of the soil surrounding the pile.

Calculation Phases

In short, the following four steps are taken to solve the complete process from installation via consolidation to pile loading for the installation of one (open-ended) displacement pile:

1. The kinematics in the soil due to pile installation are calculated using the shallow strain-path method in COMSOL, where the elliptic integrals of the first and second kind are approximated with a power series.

2. For each point in space, the strain paths of Step 1 are parsed to a strain driver in which the Creep-SCLAY1S constitutive model is implemented. This step circumvents any mesh distortion effects for the pile installation process. Given the viscoplastic model formulation, a strain rate needs to be defined. In this case, a pile penetration rate of 40 mm/s was used. This value approximates the relatively fast rate corresponding to pile installation in soft sensitive clays as encountered on the Onsøy test site.
3. The stress increments and updated state variables calculated in Step 2 are parsed back to a fully coupled 2D FE code with the Creep-SCLAY1S model to calculate the stress equilibrium, strain compatibility, and excess pore pressures (and dissipation) for the complete domain.
4. The increase of shear strength is probed numerically at several stages during the pile-setup and aging period, during which the system further evolves during consolidation and creep. An interface shear traction is applied using displacement control at 10^{-5} m/s to calculate the emerging undrained shear strength after preset periods of aging (up to 100 months after pile installation).

Although the preceding method was originally developed to model aging effects of the shaft resistance component of axially loaded piles, it principally can be extended to other cases. Depending on the loading direction and the details of the pile, this requires modification of calculation Steps 3 and 4.

Validation at Field Scale

Onsøy Pile Load Tests

Steel open-ended piles with an outer pile radius R_{pile} of 254 mm, wall thickness t of 6.3 mm, and length of 19 m have been used in the pile-aging tests performed at the Onsøy test site (Karlsrud et al. 2014). The capacity as function of time was tested using pile load tests in tension on independent piles to isolate the aging effects at the pile–soil interface. For soft soils, the failure mechanism is expected in the soil close to the pile. Hence, the measured increase in pile head capacity in tension reported is directly related to the increase of undrained shear strength in the soil adjacent to the pile shaft.

The plugging ratio during pile installation was 0.13–0.22. At this stage, a partially plugged pile cannot be directly modeled with the SSPM. As a result both the fully open-ended pile and closed-ended pile scenarios are studied, with largest gains in capacity expected for the pile installation process that disturbs the soil the most, i.e., the closed-ended piles. During the tests, an increase in tension capacity up to 21% after 2 years has been reported (Karlsrud et al. 2014). The soil properties at the Onsøy test site are well documented and have been reported by Lunne et al. (2003) and Jostad and Berre (2010).

Numerical Model

The SSPM equations are solved for two cases: (1) closed-ended pile with radius R_{pile}, and (2) open-ended pile (unplugged) with outer radius R_{pile} and wall thickness t. In the current calculations, a steady-state solution is reached for a penetration depth of 5 m. The width of the domain was chosen to be $200R_{pile}$.

The mesh and boundary conditions used for the axisymmetric pile-aging calculations and shear-strength probing consists of 2,000 quadrilateral elements with quadratic shape functions. The largest elements are positioned at the center of the model, and the element size gradually decreases to 5×10 mm (height × width) elements near the pile wall ($r = 0.254$ m) and outflow boundary ($r = 50.8$ m). Fig. 1 shows all details of the geometry and boundary conditions applied. A sensitivity study showed that the large elements at the center of the domain do not affect the results significantly. The stress states and state variables calculated with the strain driver are used as initial state. These are constant with depth, but varying with radial distance from the pile because SSPM is 1D and the part of soil adjacent to the shaft considered in the follow up calculations is only a slice 50-mm thick at 7 m depth (for which most high-quality laboratory data on block samples were available). The hydraulic boundaries are impermeable with exception of the far right boundary, which accommodates flow by prescribing a zero excess pore pressure. A similar quasi-1D approach has successfully been used by Basu et al. (2014).

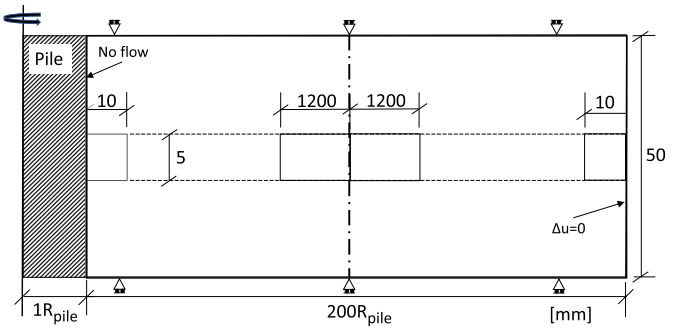

Fig. 1. Numerical domain. The element size gradually increases to $1{,}200 \times 5$ mm elements (height × width) near the center ($r = 100R_{pile}$). Not to scale.

Numerical Results

The large distortion in the clay adjacent to the pile during the installation leads to excess pore pressures, which subsequently dissipate over time. Fig. 2 shows the evolution of the excess pore pressures Δu, mean effective stress p', and deviatoric stress q as a function of time. All stress components are normalized with the far-field mean effective stress p'_o. Figs. 2(a and b) show the results for the closed-ended pile at the interface R_{pile} and $3R_{pile}$, respectively, and Figs. 2(c and d) show the results for the open-ended pile at equal distances. The closed-ended pile, where more pile volume is penetrated into the soil, leads to larger initial excess pore pressures Δu that consequently dissipate over a larger period of time ($\Delta u < 6$ kPa after 60 days) when compared with the open-ended pile ($\Delta u < 1$ kPa after 10 days).

The initial increase in the excess pore pressures after installation of the closed-ended pile is a classic case of the Mandel-Cryer effect, when due to effective stress–driven contraction of the outer annulus of soil, additional stress is generated within this annulus [Gibson et al. (1963) made the first experimental observations of this classic mechanism]. The Mandel-Cryer effect is only fully resolved in the analyses by using the complete 3D formulation of the Biot consolidation equations and the particular boundary conditions with only the far-field boundary being open. The effect is more pronounced for soft soils with low Poisson ratios $\nu < 0.2$ (Cryer 1963). Finally, for the open-ended pile, the influence radius is rather small because the effects of the installation are benign at $3R_{pile}$ [Fig. 2d)]. The spatial distribution of the changes in stress and pore pressures are further evaluated in Figs. 3 and 4 for relevant instances of time.

The stress and strain distribution in the clay adjacent to the pile are presented for the situation directly after pile installation ($t = 0$ days) and after 10, 30 (open-ended pile only), and 60 days (closed-ended pile only), and 2 years. Fig. 3 presents the results for

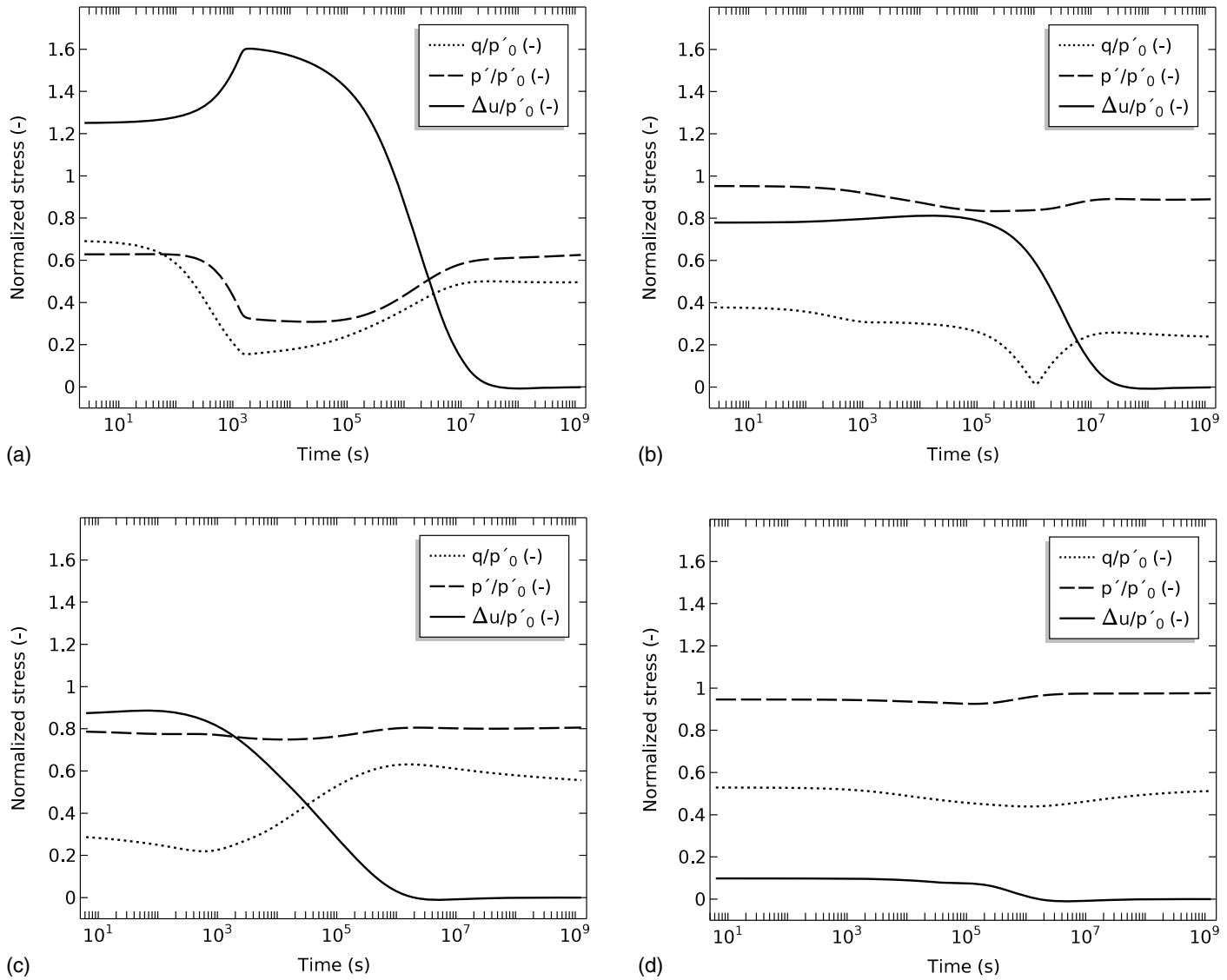

Fig. 2. Normalized mean effective stress p'/p_o, deviatoric stress q'/p_o, and excess pore pressure $\Delta u/p_o$ evolution with time at two different distances from the pile wall, where $r = 0$ is the center of the pile and $p_0 = 35.3$ kPa: (a) closed-ended pile, distance $= R_{\text{pile}}$; (b) closed-ended pile, distance $= 3R_{\text{pile}}$; (c) open-ended pile, distance $= R_{\text{pile}}$; and (d) open-ended pile, distance $= 3R_{\text{pile}}$.

the installation of the closed-ended pile, and Fig. 4 presents the results for the open-ended pile. The results are decomposed into the volumetric and deviatoric soil response. Each figure contains four subplots, with two dedicated to the volumetric response (one plot each for volumetric strain ε_v and mean effective stress p' and for excess pore pressures Δu), and the two other plots present the response in shear (deviatoric strain ε_q and deviatoric stress q). For ease of comparison, all the stresses are normalized on the far-field mean effective stress $p_0' = 35.3$ kPa.

Directly after installation, the mean effective stress p' is strongly reduced to $0.6p_0'$ and $0.8p_0'$, respectively, for the closed-ended and open-ended pile [Figs. 3(a) and 4(a)], due to the generation of excess pore pressures (shown in same figures on the second y-axis). The latter dissipate over time, leading to an increase of effective stress (with exception of the initial increase from the Mandel-Cryer effect for the close-ended pile near the interface). During this classical setup phenomenon, contractive volumetric strains occur [Figs. 3(c) and 4(c)]. In the current calculations this setup phase is predicted to be up to 60 days for the close-ended pile and as short as 10 days for the open-ended pile. These findings are similar to those presented elsewhere, where the largest soil displacement results in the largest increase in excess pore pressures (with longest dissipation time) (e.g., Randolph et al. 1979; Gourvenec and Randolph 2011). During the pile-setup stage, the stresses smooth out over a larger soil volume, e.g., Figs. 3(b) and 4(b).

Another observation is that the installation effects reach furthest, up to $20R_{\text{pile}}$, for the closed-ended pile. In this zone, the degree of damage [Figs. 3(c) and 4(c)], i.e., the amount of bonding χ of the initial intact clay left, is gradually increasing from completely remolded, $\chi = 0$, near the pile wall to largely intact, $\chi = \chi_0 = 10$, at a distance of $20R_{\text{pile}}$. The open-ended pile has a smaller influence radius, $5R_{\text{pile}}$, with more pronounced effects close to the pile wall. In addition, after installation, some bonding is still left, $\chi = 3.5$. Also, in both cases this damage is primarily occurring during the pile installation stage.

More interestingly, after dissipation of the excess pore pressures, a further effective-stress equalization occurs during ongoing creep and relaxation mechanisms (depending on the distance r). The reduced effective-stress magnitudes close to the

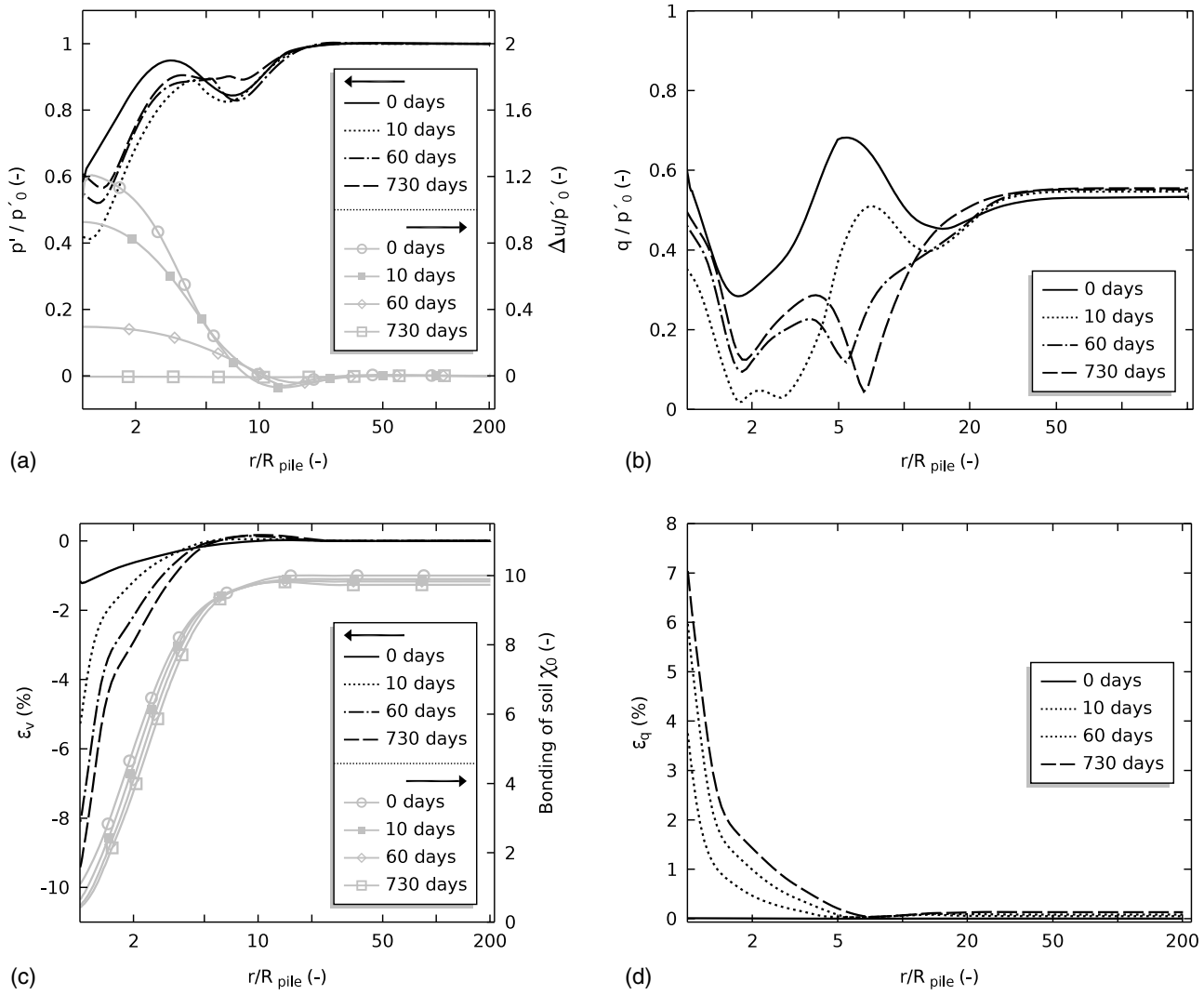

Fig. 3. Normalized stress and strain distribution as function of normalized distance from the pile r/R_{pile} at 0, 30, and 730 days after pile installation for the closed-ended pile. A logarithmic scale is used on the x-axis, and $p_0' = 35.3$ kPa: (a) normalized mean effectives stress p'/p_o' and excess pore pressure $\Delta u/p_o'$; (b) normalized deviatoric stress q'/p_o; (c) volumetric strain ε_v and bonding amount χ; and (d) deviatoric strain ε_q.

wall, $r = 1.5R_{\text{pile}}$, continue to increase slowly, leveling out to the stresses in the zone adjacent. As shown in the strain plots [Figs. 3(c and d) and 4(c and d)], this is largely a deviatoric process, as opposed to the pile setup, which is mainly a volumetric soil response.

The change in the undrained strength over time, or strength recovery, at the interface is obtained from the calculated peak resistance during application of the shear traction. The results presented in Fig. 5 are normalized with the interface shear strength at 30 days after installation in order to compare the results with the field measurements. The complementary horizontal time axis is shifted with the reference time $t_{\text{ref}} = 30$ days (1 month) corresponding to this reference strength. In the figure, $Q_{sf;\text{ref}}$ is the shaft capacity at $t_{\text{ref}} = 1$ month, and $Q_{sf;1}$ is the reference capacity 1 month after pile installation. Five data series are plotted: the measurement data (diamonds) and proposed fit from Karlsrud et al. (2014), the calculated gain in capacity for the closed-ended (solid circle) and open-ended pile (open circle), and their weighted average. The normalization with the 30 days capacity means that for the closed-ended pile simulations, a part of the increase in strength is associated with the dissipation of excess pore-water pressures, as shown in Fig. 3(a).

A strength increase between 9% (open-ended) and 56% (closed-ended) after 24 months is predicted, which bounds the 21% found in the field tests. The plugging ratios reported by Karlsrud et al. (2014) ranged between 0.13 and 0.22, which indicates neither open-ended (fully cored) nor fully closed-ended (plugged) installation. Most probably, the pile was initially open-ended during installation, with a gradual buildup of the plug at larger penetration depths. Hence, assuming a representative plugging ratio of 0.2 for all piles and that the stress-normalized results hold along the full pile length, the normalized strength gain of the field test can be further approximated by calculating the plugging-ratio weighted average of the simulated results for the open-ended and closed-ended piles. For the current simulations, the averaged strength increase is 19% after 24 months. The series of the weighted average is plotted in Fig. 5 and shows a good agreement with the measured data. The numerical simulations show a faster flattening of the curve compared with the trend line originally proposed by Karlsrud et al. (2014) and more closely resemble the expected asymptotic behavior of this process.

The main finding is that the increase in capacity over time can be modeled with good accuracy by explicitly modeling the installation

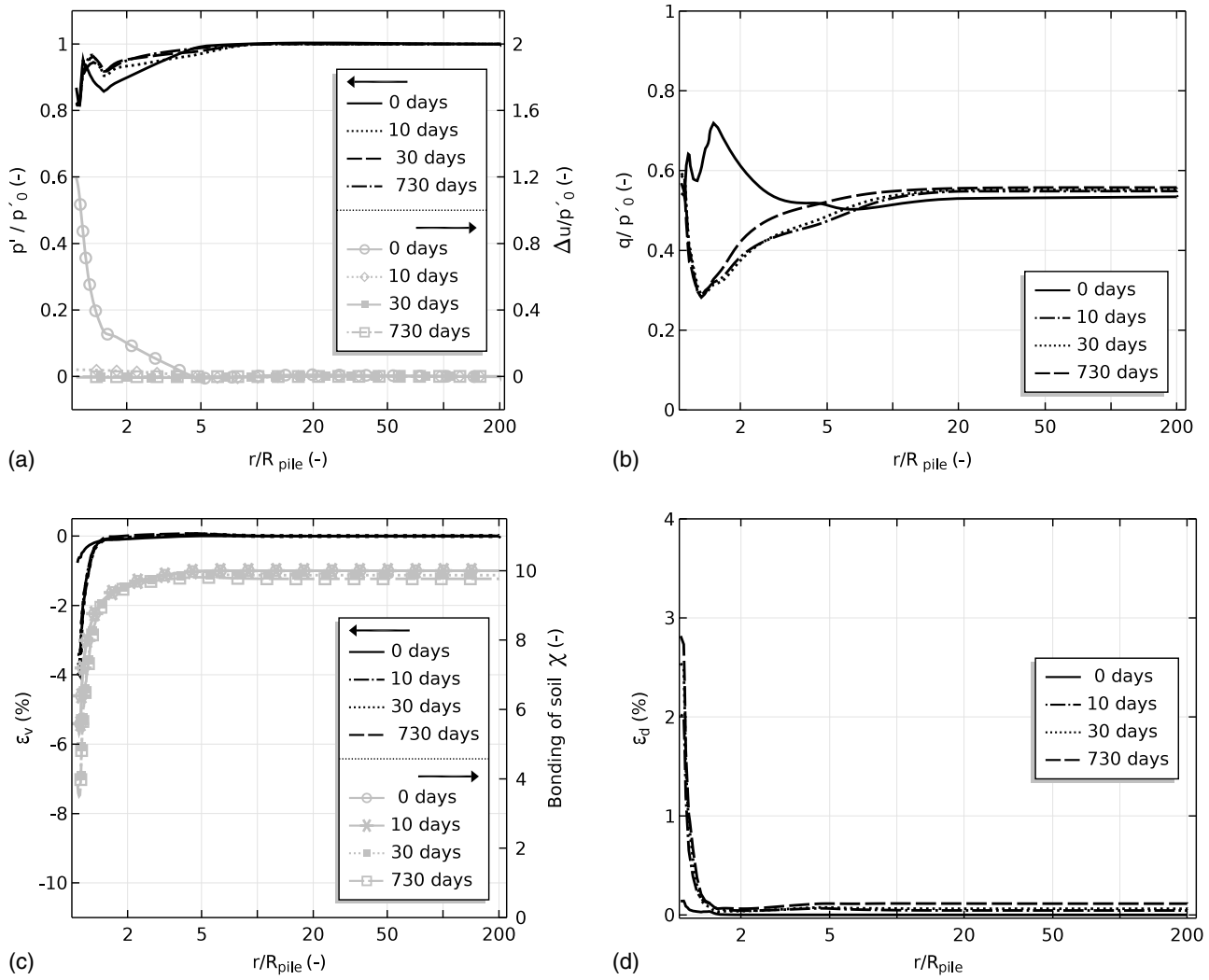

Fig. 4. Normalized stress and strain distribution as function of normalized distance from the pile r/R_{pile} at 0, 30, and 730 days after pile installation for the open-ended pile. A logarithmic scale is used on the x-axis, and $p_0 = 35.3$ kPa: (a) normalized mean effectives stress p'/p_o and excess pore pressure $\Delta u/p_o'$; (b) normalized deviatoric stress q'/p_o; (c) volumetric strain ε_v and bonding amount χ; and (d) deviatoric strain ε_q.

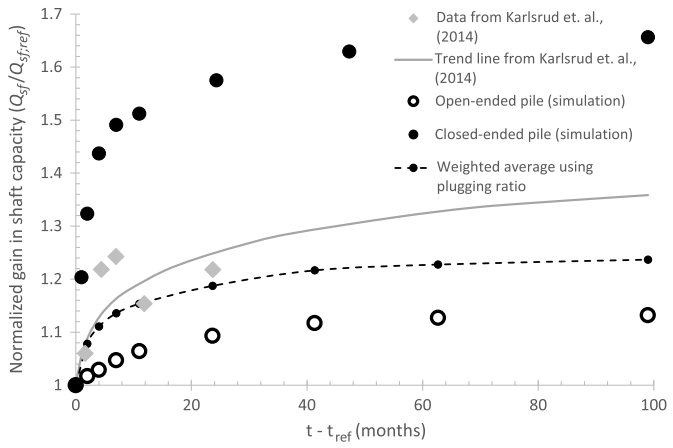

Fig. 5. Normalized gain in capacity with time using measurement data and the proposed fit from Karlsrud et al. (2014) for a simulated closed-ended pile and simulated open-ended pile. The weighted average uses a pile plugging ratio of 0.2.

process and taking into account consolidation and creep, as well as some specific soft soil features (i.e., anisotropy and the degradation of bonds). The differences remaining between simulations and measurements relate to the absence of stress redistribution in the current simulations (because only one unit length at a fixed depth is considered) and the assumption that soil governs the failure mechanism (the clay is fully bonded on the pile–soil interface).

Finally, using the model simulations, the expected increase in capacity over long periods of time (up to 100 months) show that even for the creep part of the capacity increase over time, the majority of the change occurs within the first 60 months.

It is important to highlight that especially for soft soils that display initial bonding, the simulated and measured strength increase is part of a strength recovery toward the initial strength of the intact clay before pile installation. This becomes apparent when the simulation data are replotted using the shaft capacity corresponding to the intact undrained shear strength, i.e., before pile installation, of the deposit at the depth considered for the normalization (Fig. 6). Pile installation methods that lead to smaller soil disturbance, the open-ended pile without plugging, preserve more of the initial intact strength of the soil, and therefore, a smaller strength recovery

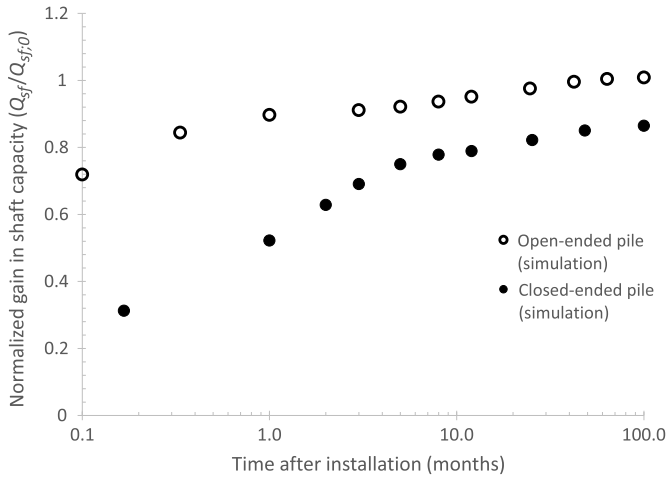

Fig. 6. Simulated gain in shaft capacity Q_{sf} with time, normalized with shaft capacity for intact clay $Q_{sf;0}$, for closed-ended and open-ended piles. $Q_{sf;0} = 32$ kPa is the shaft capacity corresponding to the intact strength of the soil before pile installation.

can be expected. For this particular situation with only moderate sensitivity, initial bonding $\chi_0 = 10$, the reduction in void ratio (contraction) during installation and pile setup almost completely compensates for the loss of strength associated with the degradation of initial bonding.

The results indicate that the open-ended tubular pile in the field test was indeed partially plugged because the measurements are bounded by the simulated results for the open-ended pile and closed-ended pile, and the weighted average is closest to the field measurements. The scatter in the measurement data suggests that the degree of plugging, and hence pile-setup time, varied between the piles tested. The second and third measured data points perhaps did not fully dissipate the excess pore pressures from installation.

Given the good performance of the proposed modeling approach, it seems likely that the governing mechanism for pile aging, the increase in capacity over time, of displacement piles driven in soft soils observed in the field relates to the stress-history dependent creep and relaxation processes in the soil adjacent to the pile shaft. This corroborates the conclusions of Schmertmann (1991), where the strengthening effects are primarily frictional, i.e., the locked-in stress at the particle level is gradually released. For piles, this leads to the redistribution of macroscopic stresses in the soil surrounding the pile. Strengthening mechanisms governed by chemical and/or biological cementation processes, such as those leading to weak bonding in the undisturbed clay, are of secondary importance for the time periods investigated. The main part of the stress-history dependence of this mechanism is governed by the large soil deformations from pile installation and the subsequent dissipation of excess pore pressures (equalization). In sensitive soft soils, this strength increase is better described as a strength recovery.

Conclusions

The effects of pile aging, namely the ongoing increase in shaft capacity after pile installation and the equalization of excess pore pressures, in soft soils can be modeled successfully by combining SSPM to model pile installation with an advanced rate-dependent (creep) model to include time-dependent effects and degradation of strength. The applicability of the proposed modeling approach was validated against a well-documented field case on the Onsøy test site. The results indicated that a large part of pile aging is governed by the creep in the soft soil surrounding the pile.

The gain in the shaft capacity in soft sensitive clays as governed by the undrained shear strength of the soil surrounding the pile is best described as a strength-recovery process toward the original intact strength before pile installation. Finally, similar to pile-setup effects that are governed by excess pore pressures, pile aging is also affected by the degree of remolding during pile installation. As a result, the amount of displaced volume, and hence the degree of strength reduction due to the pile installation, has a direct impact on the magnitude of the subsequent gain in capacity over time. Less disturbance during installation preserves more strength, which in turn leads to smaller strength recovery.

Acknowledgments

The financial support from Trafikverket in the framework Branch samverkan i Grund (BIG) and FORMAS under Contract No. 2016-01428 is greatly acknowledged.

References

Abu-Farsakh, M., F. Rosti, and A. Souri. 2015. "Evaluating pile installation and subsequent thixotropic and consolidation effects on setup by numerical simulation for full-scale pile load tests." *Can. Geotech. J.* 52 (11): 1734–1746. https://doi.org/10.1139/cgj-2014-0470.

Axelsson, G. 2000. *Long-term set-up of driven piles in sand*. Stockholm, Sweden: KTH Royal Institute of Technology.

Baligh, M. M. 1985. "Strain path method." *J. Geotech. Eng.* 111 (9): 1108–1136. https://doi.org/10.1061/(ASCE)0733-9410(1985)111:9(1108).

Basu, P., M. Prezzi, R. Salgado, and T. Chakraborty. 2014. "Shaft resistance and setup factors for piles jacked in clay." *J. Geotech. Geoenviron. Eng.* 140 (3): 04013026. https://doi.org/10.1061/(ASCE)GT.1943-5606.0001018.

Bullock, P., J. Schmertmann, M. McVay, and F. Townsend. 2005a. "Side shear setup. I: Test piles driven in Florida." *J. Geotech. Geoenviron. Eng.* 131 (3): 292–300. https://doi.org/10.1061/(ASCE)1090-0241(2005)131:3(292).

Bullock, P., J. Schmertmann, M. McVay, and F. Townsend. 2005b. "Side shear setup. II: Results from Florida test piles." *J. Geotech. Geoenviron. Eng.* 131 (3): 301–310. https://doi.org/10.1061/(ASCE)1090-0241(2005)131:3(301).

Chow, F., R. Jardine, F. Brucy, and J. Nauroy. 1998. "Effects of time on capacity of pipe piles in dense marine sand." *J. Geotech. Geoenviron. Eng.* 124 (3): 254–264. https://doi.org/10.1061/(ASCE)1090-0241(1998)124:3(254).

Cryer, C. 1963. "A comparison of the three-dimensional consolidation theories of Biot and Terzaghi." *Q. J. Mech. Appl. Math.* 16 (4): 401–412. https://doi.org/10.1093/qjmam/16.4.401.

Fellenius, B. 2008. "Effective stress analysis and set-up for shaft capacity of piles in clay." In *Research to practice in geotechnical engineering*, edited by J. E. Lair, D. K. Crapps, and M. H. Hussein, 384–406. Reston, VA: ASCE.

Fleming, K., A. Weltman, K. Elson, and M. Randolph. 2008. *Piling engineering*. New York: Taylor & Francis.

Gibson, R., K. Knight, and P. Taylor. 1963. "A critical experiments to examine theories of three-dimensional consolidation." In *Proc., European Conf. on Soil Mechanics*, 69–76. Essen, Germany: Deutsche Gesellschaft für Erd-und Grundbau e.V.

Gourvenec, S., and M. Randolph. 2011. *Offshore geotechnical engineering*. Boca Raton, FL: CRC Press.

Gras, J.-P., N. Sivasithamparam, M. Karstunen, and J. Dijkstra. 2017. "Strategy for consistent model parameter calibration for soft soils using multi-objective optimisation." *Comput. Geotech.* 90 (Oct): 164–175. https://doi.org/10.1016/j.compgeo.2017.06.006.

Gras, J.-P., N. Sivasithamparam, M. Karstunen, and J. Dijkstra. 2018. "Permissible range of model parameters for natural fine-grained materials." *Acta Geotech.* 13 (2): 387–398. https://doi.org/10.1007/s11440-017-0553-1.

Haque, M., M. Abu-Farsakh, and C. Tsai. 2016. "Field investigation to evaluate the effects of pile installation sequence on pile setup behavior for instrumented test piles." *Geotech. Test. J.* 39 (5): 20140259. https://doi.org/10.1520/GTJ20140259.

Hunt, C. E., J. M. Pestana, J. D. Bray, and M. Riemer. 2002. "Effect of pile driving on static and dynamic properties of soft clay." *J. Geotech. Geoenviron. Eng.* 128 (1): 13–24. https://doi.org/10.1061/(ASCE)1090-0241(2002)128:1(13).

Jostad, H., and T. Berre. 2010. *Additional tests on block samples in connection with the Onsøy test fill*. Technical Rep. Oslo, Norway: Norwegian Geotechnical Institute.

Karlsrud, K., T.-G. Jensen, E. K. W. Lied, F. Nowacki, and A. Simonsen. 2014. "Significant ageing effects for axially loaded piles in sand and clay verified by new field load tests." In *Proc., Offshore Technology Conf.* Red Hook, NY: Curran Associates.

Lehane, B., and R. Jardine. 1994. "Displacement-pile behaviour in a soft marine clay." *Can. Geotech. J.* 31 (2): 181–191. https://doi.org/10.1139/t94-024.

Lim, J., and B. Lehane. 2014. "Characterisation of the effects of time on the shaft friction of displacement piles in sand." *Géotechnique* 64 (6): 476–485. https://doi.org/10.1680/geot.13.P.220.

Lunne, T., M. Long, and C. Forsberg. 2003. "Characterisation and engineering properties of Onsøy clay." In Vol. 1 of *Characterisation and engineering properties of natural soils*, 395–427. Lisse, Netherlands: Swets and Zeitlinger.

Michalowski, R., and S. Nadukuru. 2012. "Static fatigue, time effects, and delayed increase in penetration resistance after dynamic compaction of sands." *J. Geotech. Geoenviron. Eng.* 138 (5): 564–574. https://doi.org/10.1061/(ASCE)GT.1943-5606.0000611.

Niemunis, A. 2008. *Incremental driver user's manual*. Karlsruhe, Germany: Univ. of Karlsruhe.

Randolph, M. F., J. Carter, and C. Wroth. 1979. "Driven piles in clay the effects of installation and subsequent consolidation." *Géotechnique* 29 (4): 361–393. https://doi.org/10.1680/geot.1979.29.4.361.

Sagaseta, C., A. J. Whittle, and M. Santagata. 1997. "Deformation analysis of shallow penetration in clay." *Int. J. Num. Anal. Methods Geomech.* 21 (10): 687–719. https://doi.org/10.1002/(SICI)1096-9853(199710)21:10<687::AID-NAG897>3.0.CO;2-3.

Schmertmann, J. 1991. "The mechanical aging of soils." *J. Geotech. Eng.* 117 (9): 1288–1330. https://doi.org/10.1061/(ASCE)0733-9410(1991)117:9(1288).

Seng, S., and H. Tanaka. 2012. "Properties of very soft clays: A study of thixotropic hardening and behavior under low consolidation pressure." *Soils Found.* 52 (2): 335–345. https://doi.org/10.1016/j.sandf.2012.02.010.

Sivasithamparam, N., M. Karstunen, and P. Bonnier. 2015. "Modelling creep behaviour of anisotropic soft soils." *Comput. Geotech.* 69 (Sep): 46–57. https://doi.org/10.1016/j.compgeo.2015.04.015.

Skov, R., and H. Denver. 1988. "Time-dependence of bearing capacity of piles." In *Proc., 3rd Int. Conf. on the Application of Stress-Wave Theory to Piles*, 879–888. Richmond, BC, Canada: The Canadian Geotechnical Society.

Whittle, A., and T. Sutabutr. 1999. "Prediction of pile setup in clay." *Transp. Res. Rec.* 1663 (1): 33–40. https://doi.org/10.3141/1663-05.

Wichtmann, T., K. Andersen, M. Sjursen, and T. Berre. 2013. "Cyclic tests on high-quality undisturbed block samples of soft marine Norwegian clay." *Can. Geotech. J.* 50 (4): 400–412. https://doi.org/10.1139/cgj-2011-0390.

Yang, L., and R. Liang. 2006. "Incorporating set-up into reliability-based design of driven piles in clay." *Can. Geotech. J.* 43 (9): 946–955. https://doi.org/10.1139/t06-054.